ACS APPLIED MATERIALS & INTERFACES

Research Article

www.acsami.org

Bioinspired Underwater Superoleophobic Membrane Based on a Graphene Oxide Coated Wire Mesh for Efficient Oil/Water Separation

Yu-Qing Liu,[†] Yong-Lai Zhang,*[,†] Xiu-Yan Fu,[†] and Hong-Bo Sun*[,†,‡]

[†]State Key Laboratory on Integrated Optoelectronics, College of Electronic Science and Engineering, and [‡]College of Physics, Jilin University, 2699 Qianjin Street, Changchun 130012, China

Supporting Information

ABSTRACT: Inspired from fish scales that exhibit unique underwater superoleophobicity because of the presence of micronanostructures and hydrophilic slime on their surface, we reported here the facile fabrication of underwater superoleophobic membranes by coating a layer of graphene oxide (GO) on commercially available wire meshes with tunable pore sizes. Using the wire mesh as a ready-made mask, GO-embellished mesh with open apertures (GO@mesh) could be readily fabricated after subsequent O_2 plasma treatments from the back side. Interestingly, the congenital microstructures of the crossed microwires in combination with the abundant hydrophilic oxygen-containing groups of the GO layer endow the resultant GO@mesh with unique underwater superoleophobic properties. The antioil tests show that the underwater contact angles of various oils including both organic reagents (undissolved in water) and vegetable oil on GO@mesh exceed 150°, indicating the superoleophobic nature. In a representative experiment, a mixture of bean oil and water that imitates culinary sewage has been well separated with the help of our GO@mesh. GO-embellished wire meshes may find broad applications in sewage purification, especially for the treatment of oil contaminations.

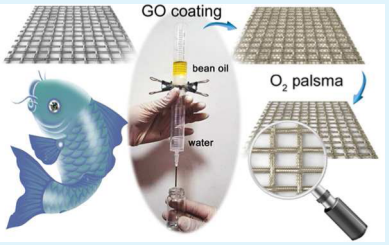

KEYWORDS: *fish scale, bioinspired, graphene oxide, underwater superoleophobic, wire mesh, oil/water separation*

1. INTRODUCTION

Nature has always been considered as the greatest scientist and engineer because natural materials not only exhibit perfect micronanostructures but also bear fascinating properties after long-time evolution. From this point of view, learning from nature is undoubtedly a shortcut to the rational design and production of artificial materials that possess multifunction similar to or even better than that of natural creatures.[1−3] In the past few decades, biomimetic fabrication has achieved great success in both fundamental science and practical applications.[4−7] For instance, the famous "lotus-leaf effect" inspired researchers to develop various superhydrophobic surfaces with self-cleaning properties;[8] the spider silk provides inspiration to design water collection microfibers;[9−11] the structure of nacre gives a hint that a layered brick-and-mortar architecture is essential to achieve superior mechanical strength and toughness;[12,13] thus, artificial materials with extraordinary mechanical properties have been successfully prepared with the help of layer-by-layer assembly.[14−16]

Recently, as learned from fish scales, which present unique underwater superoleophobicity because of water-phase micro/nanohierarchical structures, a superoleophobic and low-adhesive interface was fabricated on a solid substrate with multiscale structures via oil/water/solid three-phase systems.[17] Since then, underwater superoleophobic surfaces based on various materials have been successfully developed according to a simple principle that the superhydrophilicity of a surface at the air/solid interface is crucial to the superoleophobicity at the water/solid interface.[18−23] As a typical example, Jiang et al. coated a hydrophilic polyacrylamide hydrogel on metal mesh to prepare underwater superoleophobic membranes that could be used for oil/water separation.[19] Sun et al. fabricated hierarchical poly(dimethylsiloxane) microstructures with extreme underwater superoleophobicity by combining surface microstructures and O_2 plasma modification for the development of antioil microfluidic channels.[24] Jin et al. reported the fabrication of superhydrophilic and underwater superoleophobic poly(vinylidene difluoride) filtration membranes by grafting poly(acrylic acid) using a salt-induced phase-inversion approach.[23] Chen et al. fabricated a silicon surface that shows hierarchical micro/nanostructure by a femtosecond laser treatment.[21] Similar to fish scales, the resultant surface reveals superhydrophilicity in air and superoleophobicity underwater. However, despite the fact that underwater superoleophobic surfaces have been intensively investigated, current methods still suffer from problems with respect to complex experimental procedures or expensive materials. From a practical point of view, cost-effective and facile fabrication of underwater superoleophobic surfaces are highly desired.

As a unique hydrophilic carbon-based material, chemically exfoliated graphene oxide (GO), which can be prepared from natural graphite on a large scale, has been widely used as a precursor for the fabrication of graphene-based devices.[25−29] The presence of abundant oxygen-containing groups (OCGs)

Received: July 17, 2015
Accepted: August 21, 2015
Published: August 24, 2015

DOI: 10.1021/acsami.5b06326
ACS Appl. Mater. Interfaces 2015, 7, 20930−20936

on the GO sheets endows GO with excellent hydrophilicity, contributing to the tractable solution-processing capability. Actually, the inherent hydrophilic nature makes GO an ideal candidate for the construction of various underwater superoleophobic surfaces. In this paper, we report on the facile preparation of bioinspired underwater superoleophobic membranes by coating a GO layer on commercially available wire meshes. Similar to fish-scale structures that consist of microscale grooves and hydrophilic slime, GO-coated wire meshes also exhibit underwater superoleophobicity. The antioil property could be further optimized by tuning the mesh size. However, in spite of the superoleophobicity, the GO film on the wire meshes obturated all of the apertures. To make open pores on the GO-coated wire meshes, O_2 plasma treatment has been implemented from the back side of the mesh; in that way, the mesh structure acted as a ready-made shadow mask and a GO mesh formed on the wire mesh. The superoleophobic GO meshes reveal great potential for efficient oil/water separation.

2. RESULTS AND DISCUSSION

2.1. Fabrication of GO-Embellished Mesh with Open Apertures (GO@mesh). Scheme 1 shows a diagrammatic sketch for the fabrication procedure of GO@mesh. In a typical experiment, commercially available stainless steel wire meshes were ultrasonically rinsed in acetone to remove any organic residual on the surface. Then a GO aqueous solution, prepared by a modified Hummers' method, was drop-coated onto the mesh surface. Owing to the high viscidity of the GO precursor, a continuous GO film formed on the mesh surface after evaporation of the solvents, and thus all of the apertures have been obturated. To make open pores on the GO-coated wire meshes, an O_2 plasma treatment was implemented to the back side of the wire mesh. In this procedure, the wire mesh acted as a ready-made mask to protect the GO film underneath, and the exposed region was etched away, forming GO@mesh. The as-obtained GO@mesh samples have been directly used for subsequent experiments without any surface modifications.

Scheme 1. Diagrammatic Sketch for the Fabrication of GO@mesh

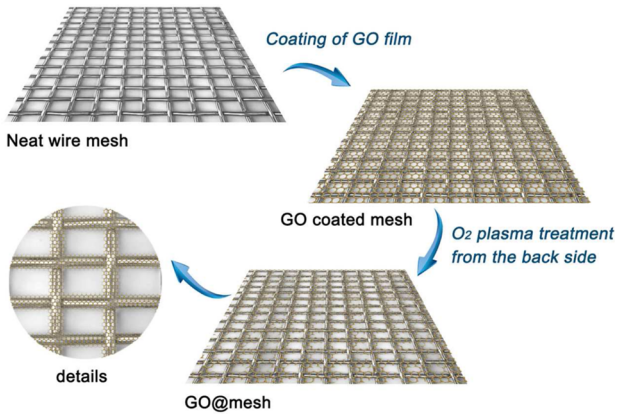

2.2. Comparison of Microstructures of Carp Scales and GO-Coated Wire Mesh. To mimic the surface topography of fish scales, we investigated the microstructures on carp scales by confocal laser scanning microscopy (CLSM). Figure 1 shows a comparison of the microstructures of fish scales and GO-coated wire mesh. The fresh fish scales were obtained from a carp (Figure 1a), and we analyzed its surface topography by CLSM. As shown in Figure 1b,c, periodically distributed grooves with an average period of ~70 μm and a groove depth of ~150 μm cover almost the entire scale. The groove structures contribute to the surface roughness, which is helpful to achieve underwater superoleophobicity. To reproduce the surface structure of the carp scale using artificial materials, we used wire mesh with different pore sizes as a template. According to the period of the microgrooves on the carp scale, GO-coated wire mesh with a mesh size of 300 shows a similar period. Figure 1d shows a photograph of the GO-coated wire mesh, which is yellow-brown in color because of the presence of the GO layer. Parts e and f of Figure 1 show the detailed surface microstructures. A continuous GO film covers the surface of the wire mesh. The interaction between GO and the mesh is van der Waals force. In our work, despite the fact that we did not modify the stainless steel wire mesh, the GO sheets attached well to the wire mesh after complete drying in air (Figure 1e). The topography of the wire mesh can be clearly

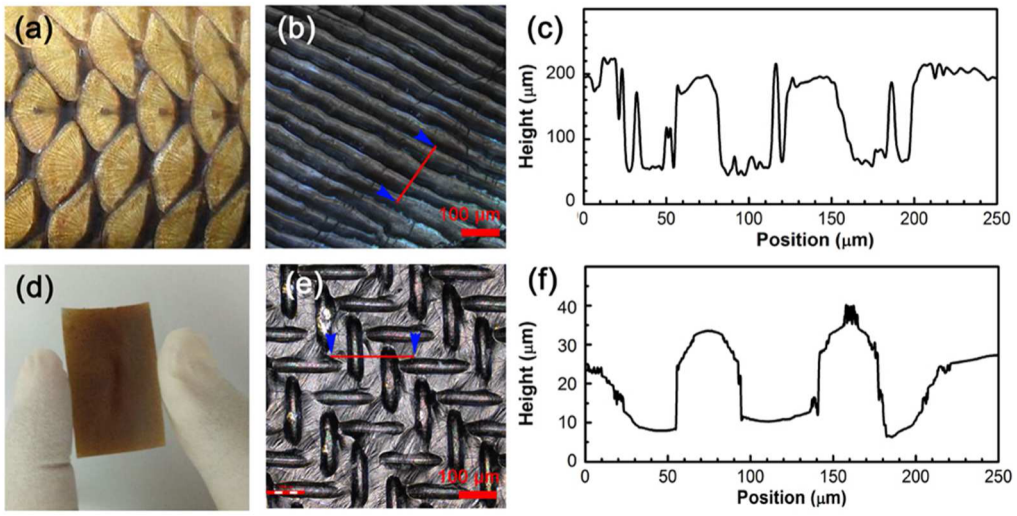

Figure 1. (a) Photograph of the fish scales. (b) CLSM image of the microstructures on a fish scale. (c) Height profile of the red line marked in part b. (d) Photograph of the GO-coated wire mesh. (e) CLSM image of the microstructures on the GO-coated wire mesh. (f) Height profile of the red line marked in part e.

DOI: 10.1021/acsami.5b06326
ACS Appl. Mater. Interfaces 2015, 7, 20930−20936

observed. Compared with the grooves on the fish scale, the roughness of the GO-coated mesh is much lower and the depth is only ~30 μm. Nevertheless, after an O_2 plasma treatment, when the pore region has been etched away, the roughness is further increased.

2.3. Role of GO. In order to expatiate the role of the GO layer, we measured the static contact angles (CAs) and the sliding angles (SAs) of a chloroform droplet on fresh fish scales and ultrasonically treated the fish scales and GO-coated fish scales, respectively. As shown in Figure 2, fresh fish scales

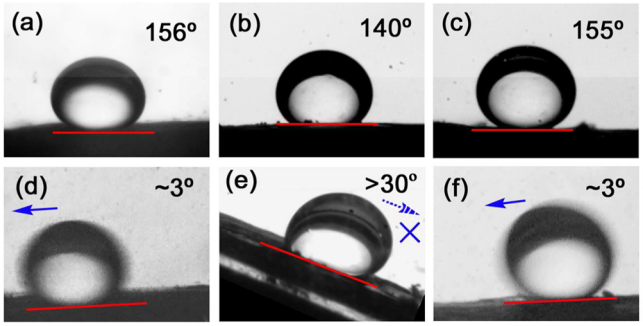

Figure 2. Underwater CAs (upper images) and SAs (bottom images) of a chloroform droplet on (a and d) fresh fish scales, (b and e) ultrasonically treated fish scales, and (c and f) GO-coated fish scales.

exhibit excellent underwater superoleophobicity; the CA is as high as 156° (Figure 2a), and the SA is only ~3° (Figure 2d), indicating the low adhesion. However, after the ultrasonic treatment, the hydrophilic slime of the fish scales has been removed, and the CA of a chloroform droplet on the surface decreased to 140° (Figure 2b), which is no longer superoleophobic. More importantly, the oil droplet pinned to the surface and could not roll away, even if the substrate has been tilted to more than 30° (Figure 2e). These results indicate that the hydrophilic slime of the fish scales plays a very important role in the underwater superoleophobicity. We further coated a thin layer of GO on the surface of the ultrasonically treated fish scales. To our surprise, the CA increased to 155° (Figure 2e), and the SA decreased to ~3° (Figure 2f). The underwater superoleophobicity recovered with the help of GO. According to these results, it is quite clear that GO with plenty of OCGs could be used as a hydrophilic coating layer to design and fabricate underwater superoleophobic surfaces.

2.4. Characterization of GO@mesh. Raman spectra of both pristine GO and the surface GO layer of GO@mesh have been collected to evaluate the structural change before and after O_2 plasma treatment. As shown in Figure 3a, two broad peaks at 1354 and 1599 cm^{-1}, corresponding to the D and G bands, could be clearly observed. Generally, the G band peak is attributed to an E_{2g} mode of graphite associated with the vibration of sp^2-bonded carbon atoms, whereas the D band peak is usually related to the vibrations of carbon atoms with dangling bonds in plane terminations of disordered graphite.[30] Notably, the I_D/I_G ratio of GO is very large, ~0.90, which indicates the presence of abundant defects on the GO sheets. After O_2 treatments, the I_D/I_G ratio further increased to ~1.15. The significantly increased D band peak is attributed to an increase in edge defects caused by the O_2 plasma treatment. In most cases, the defects could be ascribed to OCGs.

The presence of OCGs could be confirmed by Fourier transform infrared (FT-IR) spectroscopy, as shown in Figure

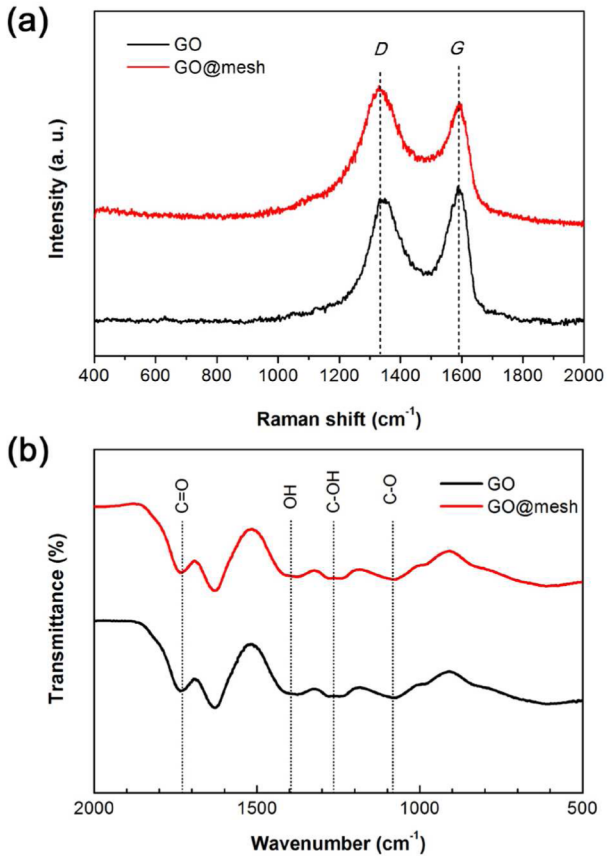

Figure 3. (a) Raman spectra of pristine GO and the GO film after an O_2 plasma treatment (GO@mesh). (b) FT-IR spectra of GO and the GO film after an O_2 plasma treatment (GO@mesh).

3b. Characteristic vibration bands include a strong C═O peak (1740 cm^{-1}), an O−H deformation peak around 1420 cm^{-1}, a C−OH stretching peak around 1230 cm^{-1}, and a C−O stretching peak around 1050 cm^{-1}, which can be clearly identified from the FT-IR spectrum of pristine GO, indicating the presence of hydroxy, epoxyl, and carboxyl groups on the GO sheets. After an O_2 plasma treatment, the FT-IR spectra remained almost the same. The presence of OCGs guarantees the hydrophilic nature of the surface GO layer on the wire mesh and contributes to the underwater superoleophobicity, accordingly.

In our experiments, the morphologies of bare wire mesh, GO-coated wire mesh, and GO@mesh have been characterized by scanning electron microscopy (SEM). As shown in Figure 4, the left column shows the SEM images of bare wire mesh with different pore sizes, which were measured to be 350, 150, 45, and 25 μm for 50, 100, 300, and 500 mesh samples, respectively. The 2000 mesh sample shows very small pores formed in the gap of microwires. After GO coating, a continuous GO film covers the entire surface. Despite the fact that the presence of the GO layer alters the surface energy of the wire mesh and leads to unique underwater oleophobicity, the apertures have been fully obturated, which limits their applications in oil/water separation. To make open pores on the GO-coated wire mesh and retain the GO coating layer on the wire surface, an O_2 plasma treatment was applied from the back side of the wire mesh. In this case, the GO film in the pore region was selectively etched away with the protection of wire meshes. The right column of Figure 4 shows the SEM images

DOI: 10.1021/acsami.5b06326
ACS Appl. Mater. Interfaces 2015, 7, 20930−20936

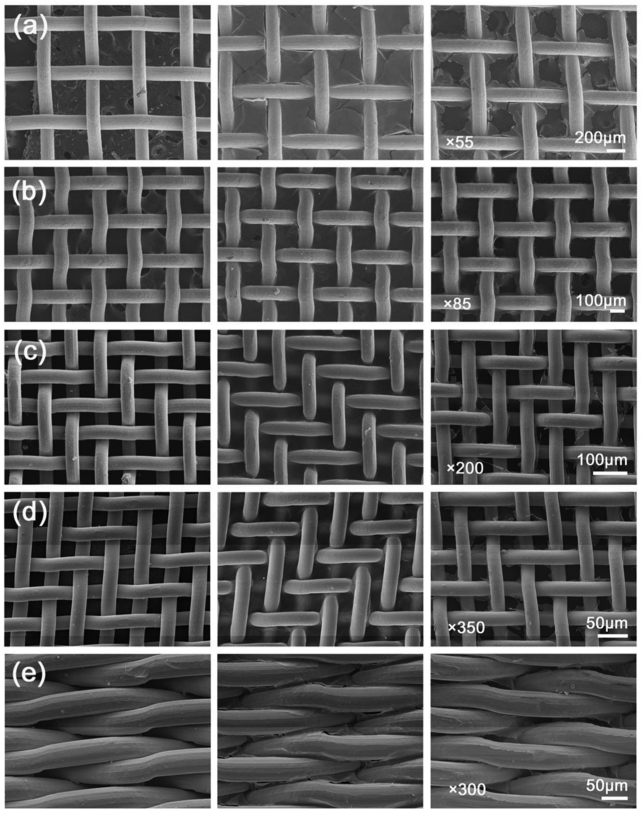

Figure 4. SEM images of bare wire meshes (left column), GO-coated wire meshes (middle column), and GO@mesh samples (right column) with a mesh sizes of (a) 50, (b) 100, (c) 300, (d) 500, and (e) 1000 mesh.

of the GO@mesh samples. Open pores can be observed from the SEM images. The GO-covered wire mesh and that after an O_2 plasma treatment (GO@mesh samples) have also been characterized by CLSM, in which the GO film could be clearly identified (Figure S1, Supporting Information).

2.5. Underwater Superoleophobicity of GO@mesh. To evaluate the underwater oleophobic properties of GO@mesh samples, we measure the static CAs of a chloroform droplet on various substrates including bare wire meshes, GO-coated meshes, and GO@mesh samples with different mesh sizes. Figure 5 shows the dependence of CAs on these substrates. Typically, before GO coating, the bare wire mesh shows relatively weak underwater oleophobicity. The CAs are in the range of 125−140°, among which the 300 mesh substrate gives the highest CAs of 140°. The relatively weak underwater oleophobicity is attributed to the hydrophobic property of stainless steel. According to Jiang et al.'s model,[17] the underwater CA of an oil droplet on the solid surface can be described by

$$\cos\theta_3 = \frac{\gamma_{o-a}\cos\theta_1 - \gamma_{w-a}\cos\theta_2}{\gamma_{o-w}}$$

where γ_{o-a} is the oil/air interface tension, θ_1 is the CA of oil in air, γ_{w-a} is the water/air interface tension, θ_2 is the CA of water in air, γ_{o-w} is oil/water interface tension, and θ_3 is the CA of oil in water. It is known that γ_{o-a} values are generally 20−30 mN·m^{-1} and γ_{w-a} is 73 mN·m^{-1}. Because θ_1 is very small, usually near 0°, and the interface tensions of the various liquids have fixed values, a decrease of θ_2 leads to larger θ_3; in other words, a more hydrophilic substrate becomes more oleophobic underwater. After GO coating, a hydrophilic GO film formed on the surface of the wire mesh. Considering the fact that GO-coated mesh still shows a similar surface topology, as discussed in Figure 2, the main change is attributed to alteration of the surface chemical composition. The presence of GO significantly decreases θ_2, as indicated by the above-mentioned equation. Obviously, the underwater CAs of chloroform increased by more than 10° for each sample. Most of the GO-coated meshes show CAs larger than 150°, indicating the superoleophobic nature. An O_2 plasma treatment was applied to create the open pores on the GO film. Because the removal of GO only occurs in the pore region, the underwater superoleophobicity does not show obvious changes. The GO@mesh-300 sample gives the highest CA of 154°. These results indicate that the GO@mesh sample with a mesh size of 300 seems to be a suitable candidate for further use in oil/water separation.

The hydrophilic property of the GO@mesh-300 sample was confirmed by CA tests. Figure 6a shows the static CA of a water droplet on the GO@mesh-300 surface. At the beginning, the CA was measured to be ~48°, indicating the hydrophilic nature. However, the CA decreased gradually because of capillary action; the water droplet could be fully adsorbed after 80 s. It is necessary to point out that the hydrophilic nature and

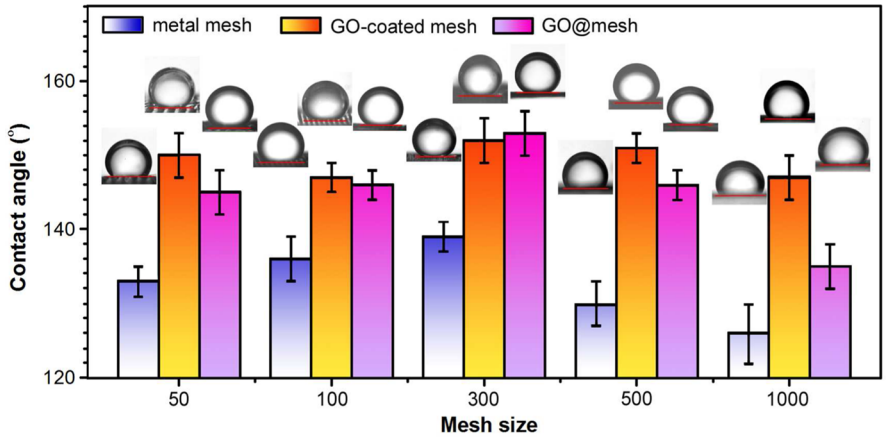

Figure 5. CAs of a chloroform droplet on bare wire meshes, GO-coated wire meshes, and GO@mesh samples with different mesh sizes. The insets are photographs of the chloroform droplet on various substrates.

DOI: 10.1021/acsami.5b06326
ACS Appl. Mater. Interfaces 2015, 7, 20930−20936

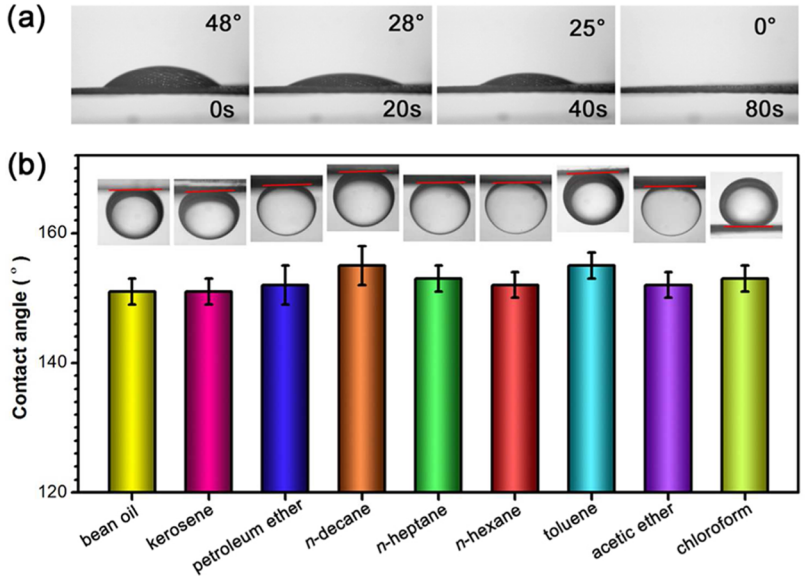

Figure 6. (a) CA of a water droplet on GO@mesh-300. The initial CA was measured to be 48°, and the CA decreased gradually because of the capillarity of the open pores. (b) CAs of different organic solvents and oils on GO@mesh-300. The insets are photographs of various droplets.

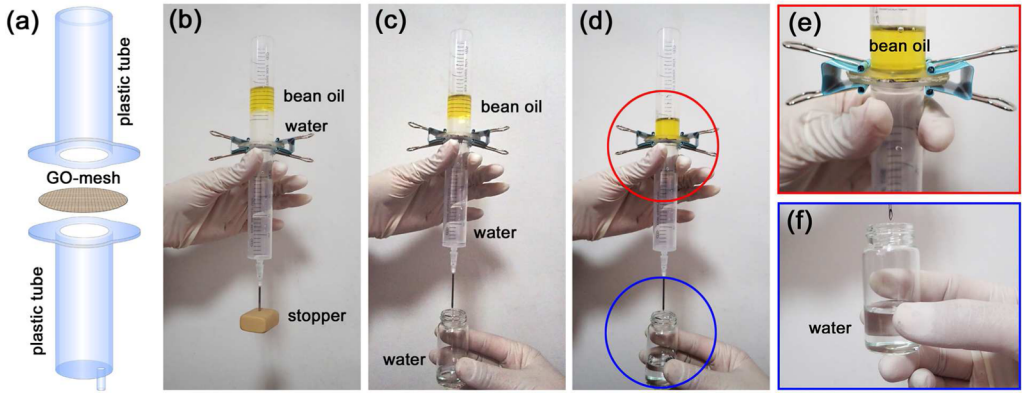

Figure 7. Oil/water separation tests using GO@mesh-300. (a) Diagrammatic sketch of the homemade device used for oil/water separation. Experimental procedure: (b) A mixture of bean oil and water was poured into the plastic tube. (c) Gravity induced drainage of the mixture. (d) Oil cannot pass GO@mesh-300, and pure water was separated from the mixture. (e) Detailed photograph of the oil/GO@mesh interface. (f) Photograph of the pure water separated from the mixture.

the aperture structures are two important factors for oil/water separation applications because the former contributes to the underwater oleophobicity, whereas the latter would guarantee the permeation of water.

To further investigate the underwater superoleophobic property of GO@mesh-300 toward other organic solvents or oils, we examine the CAs of a series of organic reagents including oil mixtures such as bean oil, kerosene, and petroleum ether and organic reagents of *n*-decane, *n*-heptane, *n*-hexane, toluene, acetic ether, and chloroform. Notably, all of these oil droplets have CAs larger than 150°, indicating the excellent underwater superoleophobic properties of GO@mesh-300. Obviously, the GO@mesh membrane does not have selectivity toward different oils, but it could be used for the efficient separation of any oil species that are insoluble in water.

2.6. Oil/Water Separation Tests. As a remediation of accidents, the cleanup of leaked oil is a global environmental issue. Compared with porous materials that have high adsorption capability,[31] oil/water separation membranes with proper dewetting properties show superior behavior because of their high separation efficiency and recycling usage. To evaluate the oil/water separation capability of the GO@mesh membrane, we prepared an oil/water separation setup. As shown in Figure 7, the GO@mesh-300 membrane was sandwiched between two plastic tubes. Then a mixture of bean oil and water (40% v/v of oil), which mimics culinary sewage, was poured into the upper tube. When the stopper was opened, water quickly permeated through the hydrophilic GO@mesh-300 and dropped into the beaker below, whereas the oil layer remained above the superoleophobic GO@mesh. The whole separation procedure was realized by gravity, and no external force was employed to the mixture. Detailed photographs show that bean oil was stopped at the oil/GO@mesh interface. The collected water was very clear with no visible oil in the water, indicating a high oil/water separation efficiency. Despite the fact that no visible oil could be detected by the naked eye, residual oil in the filtrate was extracted by ethyl acetate. On the basis of spectroscopic data, the oil content was measured to be ~0.02% by weight.

Additionally, the oil/water separation system could be reused many times. In our experiments, we found that the GO@mesh membrane works well even after recycling 50 times; no visible

DOI: 10.1021/acsami.5b06326
ACS Appl. Mater. Interfaces 2015, 7, 20930−20936

oil residuals could be detected from the filtrate. The oil content of the filtrate obtained from the 50th separation is 0.07% by weight. Moreover, we examined the surface morphology of our GO@mesh-300 membrane after oil/water separation experiments. It showed that GO sheets did not shell off, and they firmly attached to the wire mesh (Figure S2, Supporting Information), indicating its good stability. To further illustrate its durability and integrity, a rubbing test was carried out using silica spheres (~8 μm) in water. The mixture (50 mL) was forced through the membrane (GO@mesh-300, ~4 mm^2) within 1 min. After this treatment, the GO layer did not shell off (Figure S3, Supporting Information), which indicates good durability and integrity.

3. CONCLUSIONS

In conclusion, inspired from natural fish scales that possess oil repellancy in water, an underwater superoleophobic membrane was successfully prepared by coating a thin layer of the GO film on wire meshes. The crossed microwires form a rough microstructured surface, whereas the GO layer contributes to the surface hydrophilicity, similar to that of the fish-scale slime. A GO-coated wire mesh demonstrated underwater superoleophobicity. To realize open pores on the GO-coated wire mesh, an O_2 plasma treatment was applied from the back side. Using the wire mesh as a ready-made mask, the GO film in the pore region could be selectively etched away, leaving a GO mesh layer underneath. Additionally, by tuning the pore size of the wire mesh from 50 to 1000 mesh, the underwater oleophobicity could be controlled within a certain range, with the 300-mesh sample showing the best underwater antioil property. The GO@mesh-300 sample also shows underwater superoleophobicity for a wide range of oil species including oil mixtures such as bean oil, kerosene, and petroleum ether and organic reagents of *n*-decane, *n*-heptane, *n*-hexane, toluene, acetic ether, and chloroform. With the help of GO@mesh-300, we successfully realized the separation of bean oil from water. The superoleophobic GO-embellished wire meshes may hold great promise for the treatment of sewage.

4. EXPERIMENTAL SECTION

4.1. Preparation of a GO-Coated Wire Mesh. Commercially available stainless steel wire meshes with different pore sizes (from 50 to 1000 mesh) have been used for the fabrication of a biomimetic oil/water separation membrane. Fish scales were obtained from general carp. A GO aqueous solution was prepared via a modified Hummers' method by using natural graphite (Aldrich, <150 μm) as the raw material. First, the wire meshes were ultrasonically rinsed in acetone and deionized water, respectively. Then, GO was applied on the surfaces of different wire meshes by simple drop coating. The GO-coated wire meshes were dried in air at room temperature. To make open pores on the GO-coated wire meshes, O_2 plasma treatments (YZD08-2C, plasma cleaning instrument, 40 kHz, 100 W) were applied from the back side of the GO-coated meshes for 10−35 min, depending on the mesh size used. The distance between GO and the plasma source was ~5 cm. The resultant GO-coated wire meshes with open pores were denoted as GO@mesh-*x*, where *x* is the mesh size.

4.2. Characterization. The wettability and superoleophobicity of neat meshes, GO-coated meshes, and GO@mesh-*x* samples were measured by using the Contact Angle System OCA 20 (DataPhysics Instruments GmbH, Filderstadt, Germany) at ambient temperature. The CAs of various oil and organic reagents were measured with a droplet of 4 μL. SEM images were obtained by using a field-emission scanning electron microscope (JSM-7500F, JEOL, Tokyo, Japan). CLSM images were captured using a LEXT 3D measuring laser microscope (OLS4100). Raman spectra were measured with a Renishaw Raman microscope using a 514-nm-wavelength laser. FTIR spectra were performed on an IFS 66 $V{\cdot}S^{-1}$ (Bruker) IR spectrometer in the range 400−2000 cm^{-1}.

■ ASSOCIATED CONTENT

Supporting Information

The Supporting Information is available free of charge on the ACS Publications website at DOI: 10.1021/acsami.5b06326.

CLSM and SEM images of GO-coated wire meshes with diverse pore sizes (PDF)

■ AUTHOR INFORMATION

Corresponding Authors

*E-mail: yonglaizhang@jlu.edu.cn.
*E-mail: hbsun@jlu.edu.cn.

Notes

The authors declare no competing financial interest.

■ ACKNOWLEDGMENTS

The authors acknowledge the National Basic Research Program of China under Grants 2011CB013000 and 2014CB921302 and the NSFC under Grants 61376123 and 61435005 for support.

■ REFERENCES

(1) Liu, K.; Jiang, L. Bio-Inspired Design of Multiscale Structures for Function Integration. *Nano Today* **2011**, *6* (2), 155−175.

(2) Sanchez, C.; Arribart, H.; Giraud Guille, M. M. Biomimetism and Bioinspiration as Tools for the Design of Innovative Materials and Systems. *Nat. Mater.* **2005**, *4* (4), 277−288.

(3) Zhang, Y.-L.; Chen, Q.-D.; Jin, Z.; Kim, E.; Sun, H.-B. Biomimetic Graphene Films and Their Properties. *Nanoscale* **2012**, *4* (16), 4858−4869.

(4) Bai, H.; Ju, J.; Sun, R.; Chen, Y.; Zheng, Y.; Jiang, L. Controlled Fabrication and Water Collection Ability of Bioinspired Artificial Spider Silks. *Adv. Mater.* **2011**, *23* (32), 3708−3711.

(5) Jiang, H.-B.; Zhang, Y.-L.; Han, D.-D.; Xia, H.; Feng, J.; Chen, Q.-D.; Hong, Z.-R.; Sun, H.-B. Bioinspired Fabrication of Superhydrophobic Graphene Films by Two-Beam Laser Interference. *Adv. Funct. Mater.* **2014**, *24* (29), 4595−4602.

(6) Liu, Y.; Liu, J.; Li, S.; Wang, Y.; Han, Z.; Ren, L. One-step Method for Fabrication of Biomimetic Superhydrophobic Surface on Aluminum Alloy. *Colloids Surf., A* **2015**, *466*, 125−131.

(7) Zhang, Y.; Li, Z.; Zheng, Y.; Wang, J.; Song, Y.; Jiang, L. Bioinspired Fabrication Of Functional Polymer Photonic Crystals. *Gaofenzi Xuebao* **2010**, *00* (11), 1253−1261.

(8) Feng, L.; Li, S. H.; Li, Y. S.; Li, H. J.; Zhang, L. J.; Zhai, J.; Song, Y. L.; Liu, B. Q.; Jiang, L.; Zhu, D. B. Super-Hydrophobic Surfaces: From Natural to Aartificial. *Adv. Mater.* **2002**, *14* (24), 1857−1860.

(9) Bai, H.; Tian, X.; Zheng, Y.; Ju, J.; Zhao, Y.; Jiang, L. Direction Controlled Driving of Tiny Water Drops on Bioinspired Artificial Spider Silks. *Adv. Mater.* **2010**, *22* (48), 5521−5525.

(10) Ju, J.; Zheng, Y.; Jiang, L. Bioinspired One-Dimensional Materials for Directional Liquid Transport. *Acc. Chem. Res.* **2014**, *47* (8), 2342−2352.

(11) Zheng, Y.; Bai, H.; Huang, Z.; Tian, X.; Nie, F.-Q.; Zhao, Y.; Zhai, J.; Jiang, L. Directional Water Collection on Wetted Spider Silk. *Nature* **2010**, *463* (7281), 640−643.

(12) Laaksonen, P.; Walther, A.; Malho, J.-M.; Kainlauri, M.; Ikkala, O.; Linder, M. B. Genetic Engineering of Biomimetic Nanocomposites: Diblock Proteins, Graphene, and Nanofibrillated Cellulose. *Angew. Chem., Int. Ed.* **2011**, *50* (37), 8688−8691.

(13) Mayer, G. Rigid biological systems as models for synthetic composites. *Science* **2005**, *310* (5751), 1144−1147.

(14) Ariga, K.; Ji, Q.; Hill, J. P.; Vinu, A. Coupling of Soft Technology (Layer-by-Layer Assembly) with Hard materials (Meso-

DOI: 10.1021/acsami.5b06326
ACS Appl. Mater. Interfaces 2015, 7, 20930−20936

porous Solids) to Give Hierarchic Functional Structures. *Soft Matter* **2009**, *5* (19), 3562−3571.
(15) Ariga, K.; Nakanishi, T.; Michinobu, T. Immobilization of Biomaterials to Nano-Assembled Films (Self-Assembled Monolayers, Langmuir-Blodgett Films, and Layer-by-Layer Assemblies) and Their Related Functions. *J. Nanosci. Nanotechnol.* **2006**, *6* (8), 2278−2301.
(16) Ariga, K.; Yamauchi, Y.; Rydzek, G.; Ji, Q. M.; Yonamine, Y.; Wu, K. C. -W.; Hill, J. P. Layer-by-layer Nanoarchitectonics: Invention, Innovation, and Evolution. *Chem. Lett.* **2014**, *43* (1), 36−68.
(17) Liu, M.; Wang, S.; Wei, Z.; Song, Y.; Jiang, L. Bioinspired Design of a Superoleophobic and Low Adhesive Water/Solid Interface. *Adv. Mater.* **2009**, *21* (6), 665−669.
(18) Dong, Y.; Li, J.; Shi, L.; Wang, X.; Guo, Z.; Liu, W. Underwater Superoleophobic Graphene Oxide Coated Meshes for the Separation of Oil and Water. *Chem. Commun.* **2014**, *50* (42), 5586−5589.
(19) Xue, Z.; Wang, S.; Lin, L.; Chen, L.; Liu, M.; Feng, L.; Jiang, L. A Novel Superhydrophilic and Underwater Superoleophobic Hydrogel-Coated Mesh for Oil/Water Separation. *Adv. Mater.* **2011**, *23* (37), 4270−4273.
(20) Yong, J.; Chen, F.; Yang, Q.; Du, G.; Shan, C.; Bian, H.; Farooq, U.; Hou, X. Bioinspired Transparent Underwater Superoleophobic and Anti-Oil Surfaces. *J. Mater. Chem. A* **2015**, *3* (18), 9379−9384.
(21) Yong, J.; Chen, F.; Yang, Q.; Zhang, D.; Farooq, U.; Du, G.; Hou, X. Bioinspired Underwater Superoleophobic Surface with Ultralow Oil-Adhesion Achieved by Femtosecond Laser Microfabrication. *J. Mater. Chem. A* **2014**, *2* (23), 8790−8795.
(22) Zhang, F.; Zhang, W. B.; Shi, Z.; Wang, D.; Jin, J.; Jiang, L. Nanowire-Haired Inorganic Membranes with Superhydrophilicity and Underwater Ultralow Adhesive Superoleophobicity for High-Efficiency Oil/Water Separation. *Adv. Mater.* **2013**, *25* (30), 4192−4198.
(23) Zhang, W.; Zhu, Y.; Liu, X.; Wang, D.; Li, J.; Jiang, L.; Jin, J. Salt-Induced Fabrication of Superhydrophilic and Underwater Superoleophobic PAA-g-PVDF Membranes for Effective Separation of Oil-in-Water Emulsions. *Angew. Chem., Int. Ed.* **2014**, *53* (3), 856−860.
(24) Wu, D.; Wu, S.-z.; Chen, Q.-D.; Zhao, S.; Zhang, H.; Jiao, J.; Piersol, J. A.; Wang, J.-N.; Sun, H.-B.; Jiang, L. Facile Creation of Hierarchical PDMS Microstructures with Extreme Underwater Superoleophobicity for Anti-Oil Application in Microfluidic Channels. *Lab Chip* **2011**, *11* (22), 3873−3879.
(25) Guo, L.; Zhang, Y.-L.; Han, D.-D.; Jiang, H.-B.; Wang, D.; Li, X.-B.; Xia, H.; Feng, J.; Chen, Q.-D.; Sun, H.-B. Laser-Mediated Programmable N Doping and Simultaneous Reduction of Graphene Oxides. *Adv. Opt. Mater.* **2014**, *2* (2), 120−125.
(26) Stankovich, S.; Dikin, D. A.; Piner, R. D.; Kohlhaas, K. A.; Kleinhammes, A.; Jia, Y.; Wu, Y.; Nguyen, S. T.; Ruoff, R. S. Synthesis of Graphene-Based Nanosheets via Chemical Reduction of Exfoliated Graphite Oxide. *Carbon* **2007**, *45* (7), 1558−1565.
(27) Wang, J.-N.; Shao, R.-Q.; Zhang, Y.-L.; Guo, L.; Jiang, H.-B.; Lu, D.-X.; Sun, H.-B. Biomimetic Graphene Surfaces with Superhydrophobicity and Iridescence. *Chem. - Asian J.* **2012**, *7* (2), 301−304.
(28) Wang, J.-N.; Zhang, Y.-L.; Liu, Y.; Zheng, W.; Lee, L. P.; Sun, H.-B. Recent Developments in Superhydrophobic Graphene and Graphene-Related Materials: from Preparation to Potential Applications. *Nanoscale* **2015**, *7* (16), 7101−7114.
(29) Zhang, Y.-L.; Guo, L.; Xia, H.; Chen, Q.-D.; Feng, J.; Sun, H.-B. Photoreduction of Graphene Oxides: Methods, Properties, and Applications. *Adv. Opt. Mater.* **2014**, *2* (1), 10−28.
(30) Zhang, Y.-L.; Guo, L.; Wei, S.; He, Y.-Y.; Xia, H.; Chen, Q.-D.; Sun, H.-B.; Xiao, F.-S. Direct Imprinting of Microcircuits on Graphene Oxides Film by Femtosecond Laser Reduction. *Nano Today* **2010**, *5*, 15−20.
(31) Zhang, Y.-L.; Wei, S.; Liu, F.; Du, Y.; Liu, S.; Ji, Y.; Yokoi, T.; Tatsumi, T.; Xiao, F.-S. Superhydrophobic Nanoporous Polymers as Efficient Adsorbents for Organic Compounds. *Nano Today* **2009**, *4*, 135−142.

DOI: 10.1021/acsami.5b06326
ACS Appl. Mater. Interfaces 2015, 7, 20930−20936